

Supramolecular polymerization: challenges and advantages of various methods in assessing the aggregation mechanism†

Cite this: DOI: 10.1039/c8nr08472f

Roman Vill,^a Jochen Gülcher,^a Pavel Khalatur,^{b,c} Pascal Wintergerst,^a Andreas Stoll,^a Ahmed Mourran^d and Ulrich Ziener^d

Oligothiophenes with branched alkyl end groups show distinct aggregation in organic solvents. The process of supramolecular polymerization is assessed by three different methods (UV-vis absorption and fluorescence emission spectroscopy and dynamic light scattering) to exclude artifacts. An apparent dependence of the degree of aggregation on the concentration of the oligomers is observed. Above the upper limit of concentration (a lower micromolar range for the present class of compounds), experimental data delivered conflicting results and the concentration should not therefore be exceeded. Scanning force microscopy and molecular dynamics simulations confirm the formation of one-dimensional aggregates with presumably helical arrangement of the achiral monomers.

Received 19th October 2018,
Accepted 30th November 2018

DOI: 10.1039/c8nr08472f

rsc.li/nanoscale

Introduction

Supramolecular (synthetic) polymers have been experiencing steadily increasing interest since the early 1990s.¹ Similar to classical synthetic polymers, supramolecular homo- and copolymers are described.² Apart from the fundamental research, such polymer structures are of high interest for applications in, e.g. sensing and bioimaging. Also nature takes advantage of supramolecular polymerizations. For example, actin plays a crucial role in cell motility through a dynamic process driven by polymerization and depolymerization.³ Good control over the structure formation on the nanoscale in dilute solution and in combination with, e.g. optical properties, is strongly required for fluorescent organic nanoparticles. The size and structure of these nanoparticles are engineered through steered solute nucleation and growth rates in solvent precipitation processes.⁴ Supramolecular polymers can be classified by the mechanism of formation.⁵ Based on the equilibrium characteristics between the constituting monomer units and the polymer, cooperative and non-cooperative processes are

distinguished. In the latter case, often called isodesmic polymerization, there is just one equilibrium constant K and a polymer is formed at any concentration or temperature. In cooperative processes, typically a nucleus is formed with a certain activation constant K_a and above a distinct concentration or below a certain temperature, the nucleus reaches a critical size and the polymer elongates with a higher (cooperative) or lower (anti-cooperative) constant K_c . With the decreasing height of the activation energy, a transition from the nucleation-elongation to a downhill mechanism can be found.⁶ There are various models to describe the different mechanisms. While the K_2 - K model assumes the formation of dimers as critical nuclei which then elongate, the most common for the cooperative process is given by van der Schoot.^{7,8} Many examples in the literature for both isodesmic and cooperative supramolecular polymerizations have been reported and the prevailing mechanism depends on different parameters. In a first simple consideration, plain benzene-like π - π interactions promote rather an isodesmic and hydrogen bonding as a cooperative mechanism, respectively.⁵ Further structural elements might have an impact on these interactions and will influence the aggregation mechanism. Thus, more or less significant structural variations mostly of side groups in monomer classes can cause a change from the isodesmic to the cooperative mechanism or *vice versa*. Oligo(phenylene ethynylene)s with pyridine end groups display both cooperative and isodesmic polymerization, depending on the shape of the backbone, whether it is bent or linear, respectively.⁹ Slight structural variations of simple (chiral) alkoxy side-chains in triangular corresponding oligomers drive the tran-

^aInstitute of Organic Chemistry III-Macromolecular Chemistry and Organic Materials, University of Ulm, Albert-Einstein-Allee 11, 89081 Ulm, Germany

^bInstitute of Organoelement Compounds, Russian Academy of Science, Moscow 119991, Russia

^cUlm University, Polymer Science, Albert-Einstein-Allee 47, 89081 Ulm, Germany

^dDWI-Leibniz Institute for Interactive Materials, Forckenbeckstrasse 50, D-52056 Aachen, Germany

† Electronic supplementary information (the ESI) available: Experimental details on absorption and fluorescence spectroscopy, light scattering and SFM. See DOI: 10.1039/c8nr08472f

sition from isodesmic to cooperative aggregation.¹⁰ If cytidine end groups are introduced to oligopyrenotides with structural similarities to nucleotides, a change from the cooperative to isodesmic mechanism is found.¹¹ Structure dependent self-assembly, ranging from isodesmic to highly cooperative, caused by hydrogen bonding, and the effects of π stacking, hydrophobic interactions and solvent polarity are described for benzene tricarboxamides.^{12,13} Depending on the bulkiness of the substituents, a transition from isodesmic to cooperative is found for naphthalene bisimide supramolecular homo- or copolymers.¹⁴ BODIPY derivatives with ester and amide linkages, respectively, show isodesmic behaviour based on plain π - π interactions. If in addition hydrogen bonding works, a cooperative mechanism is observed.¹⁵

Such a switch of mechanism can also be induced by co-assembly. BODIPY derivatives self-assemble isodesmically but co-assembly with anthracene promotes a highly cooperative process.¹⁶ Small structural variations of solubilizing wedges in the periphery of porphyrins lead to the self-assembly to *H* or *J* aggregates *via* the cooperative or isodesmic mechanism.¹⁷

Another highly important factor in the mechanism is displayed by the solvent. A strong dependence of the mechanism on the solvent is found for tricarboxamides.^{13,18} In the case of oligo(phenylene vinylene)s the influence of the solvent is explained by the formation of a shell around the aggregates, which stabilizes the nuclei.¹⁹ An effect of solvent polarity is also found for merocyanine dyes with dipole-dipole driven self-assembly.^{20,21} Also perylenebisimide derivatives with fluorinated side groups display a solvent dependence of the mechanism. In addition, they show extremely high equilibrium constants.²² Phenylisoxazol bearing self-assembling monomers are further examples of the solvent dependent transition of the polymerization mechanism.²³

Although concentration plays a crucial role in supramolecular polymerization, there is hardly any report on the effect of concentration on the mechanism. Perylenebisimide dimers show concentration dependent fast isodesmic growth but at a reduced growth rate a cooperative mechanism is observed, which is attributed to the folding state of the monomers.²⁴

In previous contributions, we have already reported on the self-assembly of α,ω -substituted oligothiophenes with plain branched alkyl groups in solution without specifying the mechanism of formation.^{25,26} Mostly, the mechanistic considerations are based on UV-vis absorption measurements and sometimes supported by emission spectroscopy. While the concentration of the solute is often taken as an essential parameter for the control of supramolecular polymerization regardless of the concentration range, the validity of the evaluation models is hardly questioned. Here, we show for several series of oligothiophenes in organic solvents that, depending on the concentration, absorption and emission spectroscopy can deliver different outcomes and none of the methods is completely reliable in the chosen concentration regime. The strong emission response to temperature opens the avenue for employing these materials as nanothermometers. In addition to spectroscopic methods, we used scanning force microscopy

(SFM) and atomistic simulation. These studies were mainly aimed at establishing the internal structure of the emerging aggregates. In particular, our molecular dynamics simulations provide a real opportunity to shed some light on the possible chiral supramolecular self-assemblies of α,ω -substituted oligothiophenes. Both SFM and simulation reveal the one-dimensional growth of the aggregates, resulting in fiber-like nanostructures.

Results

Experimental results

Linear oligothiophenes with branched aliphatic end groups and a sufficiently long backbone show expressed self-assembly in organic solvents. The molecular structures of the employed compounds are given in Fig. 1. In previous publications, the synthesis of the compounds is described and the nomenclature in Fig. 1 is obtained from the literature.^{27,28} The systematic branching topology of the substituents comprises dendron-like structures of the first (R_J) and second generation (R_A - R_E). In the following, the oligomers are abbreviated as R_nTR with n as the number of thiophene units and the different end groups R (see Fig. 1). The difference in their bulkiness is demonstrated by the van der Waals and molar volumes, respectively. They were calculated using the Bicerano method, which is based on electro-topological indices (Table 1).²⁹

In order to follow the aggregation process of the oligomers in solution, we employed both UV-vis spectroscopy and fluorescence emission spectroscopy as powerful tools. In the literature, often methylcyclohexane is chosen as the solvent for such self-assembly studies. The oligomers are too highly soluble in this solvent so that only solutions at the highest investigated

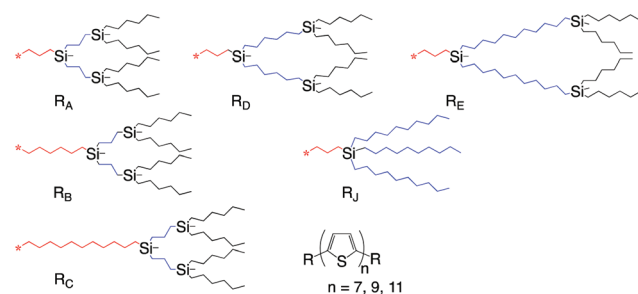


Fig. 1 Structures of the investigated oligothiophenes with varying branching topology and length of backbone.

Table 1 van der Waals and molar volumes of the respective end groups

Terminal group	vdW volume/ \AA^3	Molar volume/ \AA^3
R_A	424.9	703.7
R_B	455.5	751.9
R_C	506.4	832.3
R_D	486.1	800.2
R_E	587.9	961.0
R_J	356.6	573.0

concentration (0.4 mM) showed aggregation. Therefore, the experiments were mainly performed in another even less polar solvent, Isopar M. It is a mixture of linear and branched hydrocarbons with a boiling point above 200 °C and a freezing point below -70 °C. These data show that there is negligible evaporation and expressed aggregation for all compounds at least at higher concentrations in the accessible temperature range. In order to ensure thermodynamic control, all data points were extracted from emission spectra, which displayed a constant intensity of subsequent runs within the experimental error. Due to very slow aggregation kinetics, the thermal equilibration time for each temperature amounted to around 20 minutes. All samples were measured from high to low temperature. Due to the automated process, the UV-vis absorptions at a fixed wavelength were measured constantly within 20 min for each temperature. Exemplary full range, temperature dependent absorption spectra were recorded, too (see Fig. 2). Additionally, a few samples were investigated also from low to high temperature, where no hysteresis could be found, further emphasizing the thermodynamic control of the aggregation. The following diagram displays the exemplary absorption spectra of nonathiothiophene R_E9TR_E at 0.1 mM in Isopar M and at temperatures between 358 and 293 K (Fig. 2). It clearly shows a slightly hypsochromic shift of the maximum and the growth of a significant shoulder at *ca.* 550 nm with decreasing temperature, indicating the aggregation of the oligomers. Five isosbestic points demonstrate a high probability for the presence of an elementary process. The corresponding emission spectra at a lower concentration (0.006 mM, Fig. 3) present a strong decrease of intensity at the maximum (0-0 transition) to almost 0 with a slight increase in the long wavelength region fairly displaying one isosbestic point which makes the assumption of aggregation in an elementary process probable, too. Further emission spectra at higher concentrations are displayed in the ESI (Fig. S2†).

If for both methods the intensities at the maximum are extracted from the spectra (emission, $\lambda_{\max} = 539$ nm) or directly

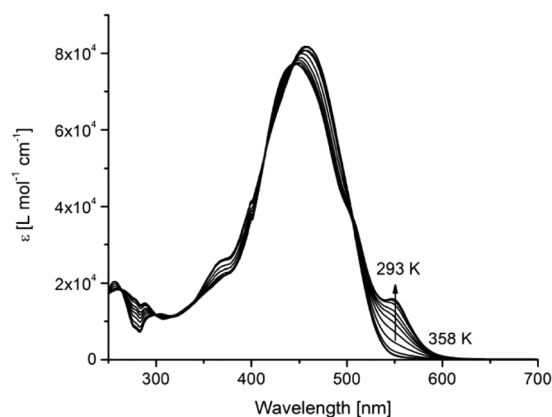


Fig. 2 Exemplary UV/Vis absorption spectra of R_E9TR_E in Isopar M (0.1 mM) at different temperatures. The arrow shows the most characteristic band developing with decreasing temperature and increasing concentration of the aggregates.

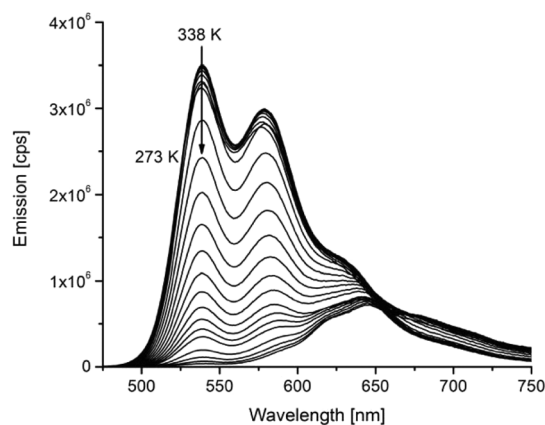


Fig. 3 Emission spectra of R_E9TR_E in Isopar M (0.006 mM) at different temperatures. The arrow shows the 0-0 transition ($\lambda_{\max} = 539$ nm) which was used to evaluate temperature dependent aggregation by decreasing the concentration of monomers and the development of the spectra with temperature, respectively.

measured (absorption, $\lambda_{\max} = 550$ nm, see Fig. S1†), respectively, the temperature dependent degree of aggregation can be derived according to $\alpha = \frac{\epsilon - \epsilon_{\min}}{\epsilon_{\max} - \epsilon_{\min}}$ (ϵ_{\max} , ϵ_{\min} : maximum and minimum absorption at the maximum of the low energy shoulder) and $\alpha = 1 - \frac{I_f - I_{f,\min}}{I_{f,\max} - I_{f,\min}}$ ($I_{f,\max}$, $I_{f,\min}$: maximum and minimum fluorescence intensities at the 0-0 transition). The formula takes into account the residual emission and absorption, respectively, of the monomers or aggregates at the respective wavelength. Fig. 4 shows a fairly good overlap of both datasets (red and black triangles, respectively). From the relatively steep increase with decreasing temperature and the non-symmetrical shape, a cooperative mechanism is assumed. It allows us to determine thermodynamic parameters accord-

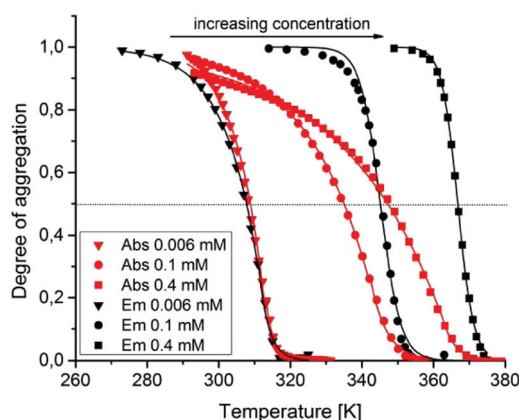


Fig. 4 Aggregation of R_E9TR_E at various concentrations derived from UV/Vis (red symbols) and emission spectra (black symbols), respectively. While emission spectra suggest a switch from the isodesmic to the cooperative mechanism with decreasing concentration, UV/Vis displays over the whole range of cooperative aggregation.

Table 2 Characteristic parameters of supramolecular polymerization for the 9 T series at $c = 0.006$ mM

Oligomer	$\Delta H/\text{kJ mol}^{-1}$	T_c/K	K_a
R _A 9TR _A	-81	295.8	4×10^{-4}
R _E 9TR _B	-88	318.7	6×10^{-4}
R _C 9TR _C	-84	344.2	5×10^{-4}
R _D 9TR _D	-80	303.8	2×10^{-3}
R _E 9TR _E (fluo)	-87	313.7	3×10^{-3}
R _E 9TR _E (UV)	-89	314.4	1×10^{-3}
R _J 9TR _J	-77	311.6	3×10^{-4}

ing to the model of van der Schoot with two branches for the nucleation and elongation regime, respectively.^{7,8} The values are in quite good agreement (Table 2, entries 5 and 6) and are in the expected range found in the literature for other oligomers in organic solution.^{8,15,21}

If the concentration is increased to 0.1 and 0.4 mM, respectively, the picture changes dramatically. From the UV-vis measurements curves for $\alpha = f(T)$ are shifted to higher temperatures as expected in comparison to the sample at low concentration (Fig. 4, red circles and squares). The still non-symmetrical shape supports a cooperative mechanism consistent over the whole concentration range. Although the data from UV-vis can be fitted nicely with hardly any kink between the two branches, a closer look at the thermodynamic data reveals fluctuating and partially much too high enthalpies in the range of some hundred kJ mol^{-1} . Additionally, there is a surprising crossing of both curves at *ca.* 320 K (see Discussion). The inconsistent data might be caused by the non-linear effects between concentration and signal intensity at relatively high concentrations. Completely different results are obtained from the emission measurements (Fig. 4, black circles and squares). Moving from 0.006 over 0.1 to 0.4 mM, there is an apparent change of the shape of the curves from non-symmetrical to highly symmetric and a sharpening of the aggregation step. These findings support an apparent change of the mechanism from cooperative to isodesmic. The data can be nicely fitted with the corresponding function, especially at the highest concentration, delivering again a surprisingly high value for ΔH (*ca.* 555 kJ mol^{-1}) and a quite small ΔT (2.22 K, derived from the fitting curve, see the ESI†). It shall be mentioned that the isosbestic point at low concentration smeared out to a broad range with increasing concentration (ESI, Fig. S2†). This is due to an overall decrease of intensity in the long wavelength region and at low temperature. Although this might indicate a decrease of total concentration by *e.g.* precipitation the solution stays visually fully transparent. Analogous measurements were performed for the compounds with different substituents and a number of thiophene units (see Fig. 1). Additionally, for two samples the solvent was changed to MCH. The following figures display the degree of aggregation determined by fluorescence spectroscopy for the 9T series at 0.006 mM in Isopar M (Fig. 5), R_E11TR_E at very low concentrations (80 and 500 nM, Fig. 6) and the 7T series at 0.4 mM (Fig. 7). As in the case of R_E9TR_E, consistently at low concen-

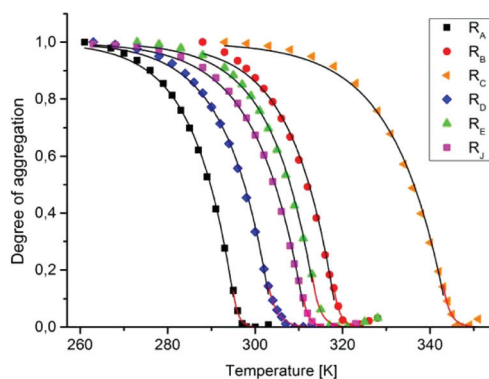


Fig. 5 Aggregation of 9 T series at low concentration (0.006 mM) displaying a cooperative mechanism of supramolecular polymerization.

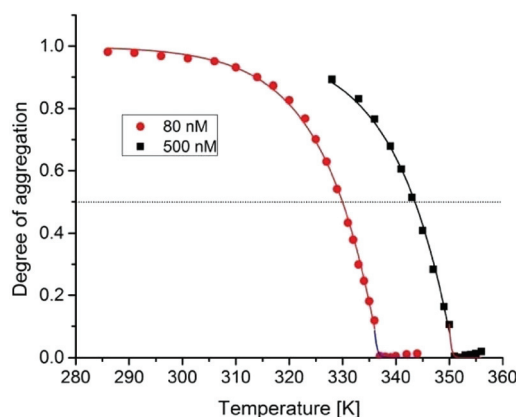


Fig. 6 Aggregation of R_E11TR_E at very low concentration (80 and 500 nM) in Isopar M with fit curves for the cooperative mechanism according to the literature.^{7,19}

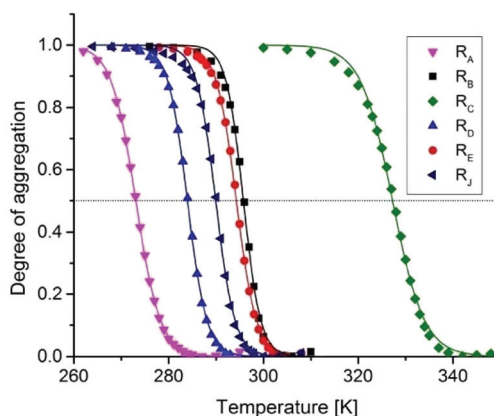


Fig. 7 Aggregation of the 7T series in Isopar M at high concentration (0.4 mM) with fit curves according to the literature.^{7,19}

trations, non-symmetrical curves are found pointing to a cooperative mechanism, while at high concentration an apparent isodesmic behaviour prevails.

Also, the change of the solvent does not alter the shape of the curve (Fig. 8).

Evaluating the “isodesmic” curves (Fig. 7 and 8) delivers enthalpic values in the range of some hundred kJ mol^{-1} and ΔT between 1.7 and 3.1 K corresponding to the results for R_E7TR_E (see above). From these curves, a transition temperature can be extracted at half height ($\alpha = 0.5$) according to the literature.⁸ Depending on the bulkiness of the branched part and the length of the spacer between the oligothiophene backbone and the first branching point, an increasing temperature from 273 K to 326 K in the order R_A (273 K) < R_D (284 K) < R_J (290 K) < R_E (294 K) < R_B (296 K) < R_C (327 K) is observed. Although the absolute values are quite different, this order is fairly in accordance with the highest transition temperatures (isotropization) in the solid state.²⁸ A slight deviation is found in the middle region, where in the solid state the order of increasing temperature is R_A (385 K) < R_J (400 K) \approx R_D (401 K) < R_E (411 K) < R_B (428 K) < R_C (469 K). This small difference is attributed to the specific effects of the additional interactions with the solvent. Thus, the influence of the different substituents on the intermolecular interactions seems to be quite comparable for both the supramolecular polymers in solution and the solid-state structures, which can be regarded as strong support of the solid-state structure, too.

Although both spectroscopies (absorption and emission) are based on the same species and electronic transitions, they deliver at high concentration quite differently shaped aggregation curves. In order to support one of both results, a third more direct method was desired. Thus, the aggregation was followed by dynamic light scattering. This was performed exemplarily for two samples at high (R_E7TR_E at $c = 0.4$ mM in Isopar M) and low concentration (R_C9TR_C at 0.006 mM in Isopar M), respectively (Fig. 9). There is a slight shift of the onset of aggregation in the low concentration case (Fig. 9a) which we attribute to the deviations of the temperature control of the two apparatus (DLS and emission spectrometer, respectively) but both datasets can be nicely fitted with the model of

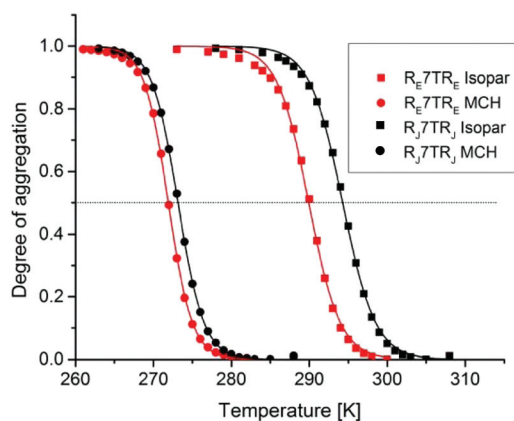


Fig. 8 Comparison of the aggregation of R_E7TR_E and R_J7TR_J at high concentration (0.4 mM) in Isopar M and methylcyclohexane, respectively.

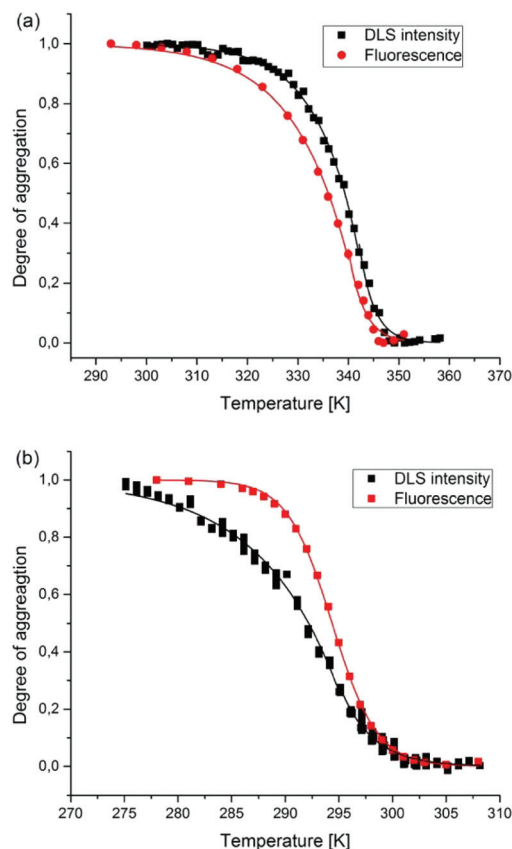


Fig. 9 Aggregation of (a) R_C9TR_C at 0.006 mM and (b) R_E7TR_E at $c = 0.4$ mM in Isopar M studied by emission spectroscopy (red) and DLS (black), respectively. Fit curves are constructed in accordance with the literature.^{7,19}

cooperative aggregation and are fairly congruent. In contrast, at high concentration both curves from DLS and fluorescence measurements differ significantly. While fluorescence delivers a sigmoidal shape (orange circles in Fig. 7 and red squares in Fig. 9b are identical) DLS clearly demonstrates that a cooperative mechanism takes place like UV-vis shows for R_E7TR_E at $c = 0.4$ mM in Fig. 4. Thus, the more reliable “true” mechanism is apparently a cooperative one regardless of the absolute concentration supported by both UV-vis and DLS measurements. Apparently, fluorescence feigns a change of mechanism which must be inherent to the method.

Although both the solvent and solute molecules are quite non-polar, a better understanding of the solvent–solute interactions can help explain the different outcomes from absorption and emission spectroscopy. Therefore, we have performed the exemplary static light scattering of R_J7TR_J in Isopar M at different concentrations. It delivers the second virial coefficient $A_2 \approx -0.02$ mL mol g^{-2} assuming a dn/dc of ca. 0.28 mL mol^{-1} (see ESI, Fig. S3†). While the absolute amounts might be somewhat inaccurate, the negative value of A_2 unambiguously demonstrates preferred oligomer–oligomer and solvent–solvent over oligomer–solvent interactions supporting a pre-

aggregation model with close oligomer–oligomer contacts which is also predicted by the simulation results (see below).

Additionally, revealing the supramolecular structure of the aggregates will further support an explanation for the concentration dependent apparent aggregation mechanisms.

Morphological control

All the findings correlate with the one-dimensional growth of the aggregates. As shown in previous publications for a 13T and 7T, fibres are formed.^{26,28,30} The corresponding structures are found for all aggregates in the present report, too. Fig. 10 displays the representative topographic images of R_E7TR_E and R_B11TR_B , acquired by scanning force microscopy, clearly showing the nanoscale fibres. The 2D fast Fourier transform of the images leads to mean interfibre distances of 5.9 nm and 5.4 nm, respectively. The width corresponds fairly to the length of a single molecule, suggesting that one-dimensional aggregates by π - π stacking are formed. Although the single fibres should display a helical structure with a defined handedness and the whole mixture should be racemic (see the next paragraph), no hints for chirality are detected in the SFM images. This is attributed to the bulky and flexible alkyl chains that interfere with the visualization of the core chirality. We also measured the optical activity of the solution in a chiral solvent by circular dichroism, but no chiral induction with preferential formation of one enantiomer could be detected.

Presumably, the influence of the chiral solvent on the core chirality is too weak.

Insightful data were provided by molecular dynamics simulation with R_J7TR_J regarding the underlying causes of directional growth and the internal structure of aggregates.

Simulation results

In this subsection, we address the problem of equilibrium aggregation (multimerization) in solutions of α,ω -substituted oligothiophenes simulated atomistically. A variety of complementary simulation methods that have been widely applied in our previous research for oligothiophene–peptide molecular hybrids³¹ were employed in the present study. Based on the simulations, we suggest the structural models both of individual molecules and supramolecular self-assemblies. These models provide the important possibility of shedding some light on the possible supramolecular organization patterns, their stability and the governing interplay of intermolecular interactions. They are also useful for understanding the aggregation mechanism at the molecular level. Unless specified otherwise, the simulated compound is triblock R_J7TR_J and the solvent is 1,1,2,2-tetrachloroethane (TCE). Although the experimental results were mainly obtained from Isopar M as the solvent, previous studies have revealed that in principle the same behaviour is found in TCE but with inappropriately shifted transition temperatures. For the simulation results the smaller TCE molecules were chosen.

From the standpoint of molecular interactions, there are two main ingredients that govern noncovalent multimerization: incompatibility of molecules and intermolecular potential. Traditional incompatible molecules (“amphiphiles”) are composed of two distinct parts – a solvophilic segment, covalently connected to a solvophobic segment. Aiming at demonstrating the incompatibility of the end-capped oligothiophene R_J7TR_J , we used the class II polymer consistent force field (PCFF)³² to calculate the Flory–Huggins interaction parameter χ of the hydrogenated groups R_J and oligothiophene segments 7T surrounded by the TCE solvent. The χ provides quantitative information on the strength of the interactions between the dissolved species and is somewhat similar to the second virial coefficient expressing binary interactions between molecules. From the predicted mixing energies E_{mix} of the binary systems and the coordination numbers Z explicitly estimated for each of the possible molecular pairs with Monte Carlo simulations, the values of χ at 298 K were found to be 1.1 and ≈ 50 for R_J and 7T, respectively. We have also tried to explore the influence of the solvent on the values of the evaluated χ parameters. When TCE was replaced with eicosane, χ values were found to be 0.53 and ≈ 46 . It seems evident that very large positive values of χ should necessarily lead to immiscibility for the oligothiophene/solvent system. In other words, the oligothiophene segments are strongly solvophobic. In contrast, the flexible-chain aliphatic end groups can be classified as moderately solvophilic and, hence, TCE is a selective good solvent for these groups which tend to be solvated.

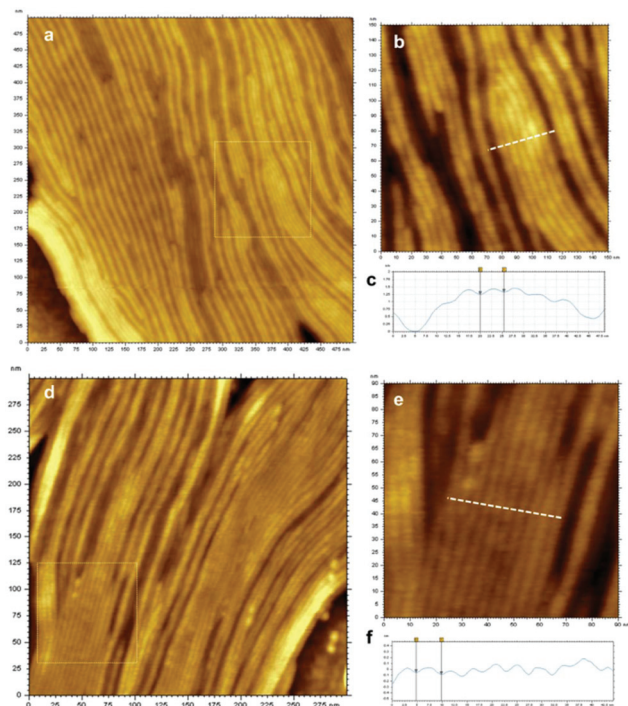


Fig. 10 Tapping mode topography images of a thin film with an average thickness of 8 nm: (a) R_E9TR_E and (b) R_B11TR_B . Thin layer prepared by spin casting of 1 g L^{-1} toluene solution onto UV- O_2 pre-cleaned SiO_2 wafer (Agilent 5500 SFM, NCH-W point probe).

By substituting the obtained temperature-dependent χ in the general expression for the free energy of mixing of a binary system,³³ the free energy was evaluated for different temperatures and solution compositions. From this, the phase diagrams were then determined. As expected, the upper critical solution temperature of the 7T/TCE system is unrealistically high, more than 1000 K, reflecting the immiscibility of the components. For the R_J/TCE solution, however, the critical point does not exist due to the small value of the χ parameter over the entire temperature range. Because the solution has no critical point, binodal and spinodal curves also do not exist. The delicate balance between the entropy term (which is calculated exactly) and the energy term (which is calculated approximately) determines the specific magnitude of the system free energy and, hence, the presence or absence of the critical temperature. Our calculation shows that the boundary delimitating these two states lies close to $\chi = 1.5$ for the R_J/TCE solution. Since the χ parameter obtained for end groups is not too different from this boundary value, we cannot exclude a weak tendency for these groups to aggregate.

Based on the performed atomistic simulations, it is possible to construct a fairly obvious simple model of end-capped oligothiophenes. In Fig. 11a, the terminal R_J group is rendered ellipsoid, covering the approximate extent of the atoms contained in this group. The size of the ellipsoid is related to the corresponding time-averaged radius of gyration R_g . Because the oligothiophene segment is actually a rigid rectilinear framework, each individual molecule can naturally be represented as a dumbbell (Fig. 11b), for which both translational and rotational movements are possible in dilute solution. It is clear that when averaged over different orientations, each symmetrical dumbbell looks like a sphere that possesses a solvo-

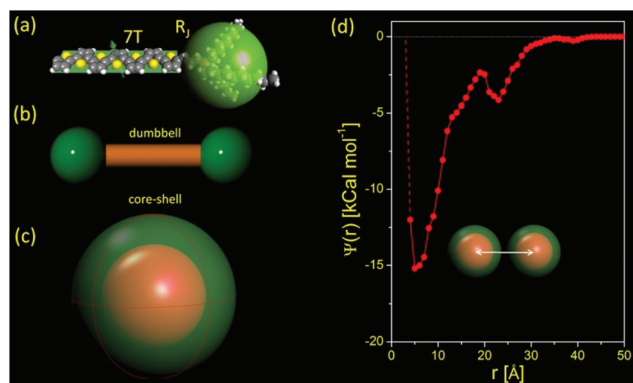


Fig. 11 (a) End-capped oligothiophene R₃7TR_J for which the only one (right) terminal group R_J is shown. Its average radius of gyration is $R_g = 20.4$ Å; the average length of the thiophene block is 23.7 Å. (b) Dumbbell, a simple model of structurally symmetric end-capped oligothiophenes. (c) Core-shell spherical model representing a dumbbell freely rotating in dilute solution. The outer shell consisting of soluble parts of the molecule provides efficient shielding of the inner thiophene segment from the solvent. (d) Intermolecular potential for molecules R₃7TR_J dissolved in TCE at 400 K calculated with atomistic MD as a function of the distance between the centers-of-mass of the molecules.

phobic core shielded from the organic solvent by a soluble aliphatic shell (Fig. 11c). However, the structural anisotropy between the diameter and length is expected to lead the dumbbells to have important additional self-organizing properties compared to their spherical counterparts. To illustrate this, we calculated the effective intermolecular potential in solution.

The intermolecular potential $\Psi(r)$ was calculated as a function of the distance r between the centers-of-mass (COM) of two oligomers placed in a large periodic box filled with TCE solvent. Using a 1 μ s GPU-accelerated molecular dynamics (MD) run performed in the NVE ensemble with the LAMMPS simulation package,³⁴ we averaged the oligomer-oligomer interaction energy at different r , taking into account that the interaction energy includes a pair component, which is defined as the pairwise energy between all pairs of atoms where one atom in the pair is in the first molecule while the other is in the second molecule. Note that the total interaction energy included the long-range coulombic contribution between all the atoms in the first molecule and all the atoms in the second molecule. The obtained time-averaged potential $\Psi(r)$ is shown in Fig. 11d.

When the COM-COM separation r is less than ≈ 50 Å, the molecules begin to attract each other. The attraction is enhanced when r is reduced up to 4 Å, thus providing conditions for the favourable π - π stacking of thiophene rings. At $r < 4$ Å, a strong sterically driven repulsion begins. An interesting result is that in the range $r \approx 20$ Å, there exists a well-pronounced energy barrier, which is due to less energetically favourable 7T-R_J interactions and interactions between 7T blocks at a nonplanar orientation of their thiophene rings. The existence of the energy barrier and the corresponding potential minimum allows us to speculate that a weak molecular pre-aggregation, which precedes the subsequent association of oligothiophenes, is possible.

The dominant factor, responsible for the self-assembly of oligothiophene-based triblocks, is the π - π stacking of inner conjugated fragments. However, owing to the relatively weak nature of the corresponding attractive forces, the resulting interplay of intermolecular interactions also suggests the dependence of the supramolecular organization on the interaction between end groups and the external conditions, such as temperature, solvent quality, *etc.* The X-ray data, available in the literature,³⁵ suggest that the unit cells of unsubstituted oligothiophenes (6T and 8T) belong to the space group $P2_1/n$ and present the herringbone packing common to a great deal of planar molecules. The distance between the nearest parallel molecular planes is 3.6 Å. It is easy to understand that two closely located end-capped molecules cannot have parallel-oriented thiophene segments because of the strong overlap of the bulky end groups and their steric repulsion. In order to weaken the overlap and maintain an energetically favourable planar conformation, the molecules have to rotate relative to each other to a certain angle φ . The MD/NVT simulations performed for molecular dimers, composed of two oligomers R₃7TR_J, demonstrated that when the average distance between thiophene planes is close to 4 Å, the average value of φ is $20 \pm 4^\circ$

at 298 K. With an elongation of the thiophene block, this angle decreases; for example, we have $\varphi = 15.3^\circ$ for R_7TR_7 at the same r . When the intermolecular distance is increased to 24 Å and more, the angle φ can take arbitrary values. These results are essential for describing the general spatial organization of the multimers being formed, but not sufficient for understanding their local structure.

The local arrangement of thiophene stacks can be understood using a simple trimer model (*cf.* Fig. 12). There are three different aggregation scenarios for compositionally symmetric α,ω -substituted oligothiophenes, depending on the rotation angle φ . As already noted, the parallel arrangement of thiophene blocks ($\varphi = 0$) is not possible for steric reasons (Fig. 12, left). Fairly strong steric conflicts also arise if we assume alternating rotations ($\pm\varphi$) of neighboring molecules: in this case, the terminal groups of the first and third molecules turn out to be close to each other (Fig. 12, right). Rotation in the same direction ($+\varphi$ or $-\varphi$) is the only possibility when thiophene blocks are strongly associated (the COM–COM separation r is close to 4 Å) and have a nearly planar conformation (Fig. 12, middle). It is clear that with this local structural motif, the aggregation process should develop in one direction, perpendicular to the long axis of the thiophene block, and lead to the formation of a right-handed or left-handed helicoidal fibril, *i.e.*, a quasi-one-dimensional chiral object. Here, it is important to stress that chiral structures are expected to arise from achiral molecules as a result of specific intermolecular interactions. To verify this, we performed atomistic MD simulations of the R_7TR_7 solution in tetrachloroethane.

Eight R_7TR_7 oligomers were placed in the simulation box with periodic boundary conditions, filled with TCE molecules at a density of 1.59 g cm⁻³. After long equilibration of the system at 300 K, we analyzed the formation of molecular aggregates of different sizes during the productive MD run. Most often, we observed the formation of dimers and trimers, but after a fairly long 200 ns simulation, the formation of an aggregate consisting of 8 molecules was also detected (*cf.* Fig. 13). In support of our model arguments, illustrated in Fig. 12, we found that the associative complexes with an aggregation number greater than 3 are indeed characterized by the presence of a helicoidal motif, *i.e.*, possess chirality with random selection of the twist direction. It is natural to expect that long

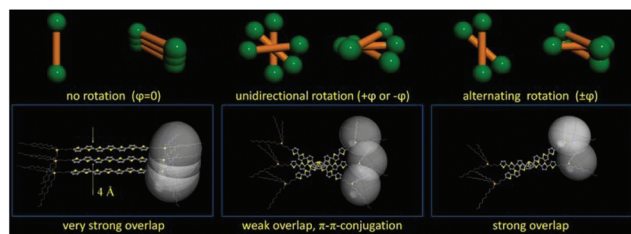


Fig. 12 Schematic representation of the aggregation scenarios expected for three self-assembling structurally symmetric α,ω -substituted oligothiophenes.

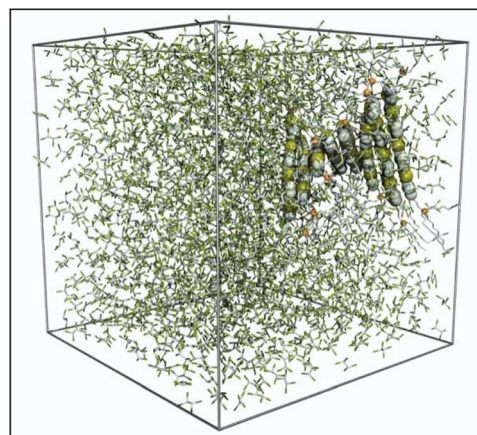


Fig. 13 Representative snapshot of the R_7TR_7 solution in TCE. Flexible-chain aliphatic terminal groups and solvent molecules are depicted by sticks, while spheres are used to render the atoms of oligothiophene segments. Hydrogen atoms are not shown.

chiral fibrils will arise in the solution with a larger number of dissolved molecules.

There is an active current search for routes to create chiral architectures from achiral molecules and for mechanisms responsible for the appearance of chirality. It is known that chiral supramolecular objects can occur if the molecules are achiral, but have a specific spatial structure/shape that makes it easier for them to pack into the twisted structures, a remarkable and rather counterintuitive collective behavior observed for banana-shaped (or boomerang-shaped) molecules,³⁶ molecularly achiral “shape incompatibles” comprising end-tethered moderate and low aspect ratio rods³⁷ and diblock rod-coil copolymers with achiral rigid and flexible blocks.³⁸ Our dumb-bell-like incompatible molecules add one more example to this list. The combination of conjugated oligothiophene blocks of different lengths with bulky end substituents provides versatile control of supramolecular organization, thus allowing the rational design of long twisted fibrils with the desired diameter and pitch of the helix. The helix can be either left- (anticlockwise) or right- (clockwise) handed, left or right-handed twist is selected randomly for every individual fibril, thereby resulting in a macroscopically achiral ensemble of aggregates each of which is homochiral.

The oligomer \leftrightarrow aggregate equilibrium in selective solvents represents a dynamic process, in which individual molecules migrate between multimer and oligomer states. As noted in the Introduction, molecular aggregation can proceed in principle by two mechanisms, which correspond to (i) the multiple equilibrium (open-aggregation or isodesmic) model of multimerization assuming a continuous growth/disintegration of the aggregates and (ii) the mass action (closed-aggregation or nucleation-growth) model of cooperative multimerization assuming a dynamic equilibrium between the molecularly dissolved oligomers and the aggregates of an optimum size.³⁹ It seems that our simulation results suggest an isodesmic route, which is independent of concentration (no critical concen-

tration for aggregate formation) and characterized by a series of equilibria between oligomers, dimers, trimers and so on, rather than a nucleation-growth self-assembly pathway. This is a typical stacking process, in which an essentially constant increment of free energy accompanies the addition of each oligomer to the end of the growing linear aggregate or the removal of the terminal molecule upon disintegration of the aggregate, a process reminiscent of linear polymerization-depolymerization. In principle, such aggregates can grow infinitely, unlike the cooperative nucleation-and-growth process, where new aggregation nuclei are formed continuously and their growth slows down as they approach an equilibrium (optimal) size, so that they can grow only to a limited size.

Unfortunately, atomistic simulations of the complete self-assembly process for the large number of R_3TR_3 molecules in solution are far beyond our computational capabilities, which are typically limited to the simulation times in the nanoseconds range while self-assembly typically happens on much larger time scales, up to seconds and even minutes as mentioned above. Therefore, we limited ourselves to the construction of multimers “manually” and the subsequent investigation of their structural properties and stability. In particular, we constructed a rather long fibrillar aggregate from the well-equilibrated trimers (like those shown in Fig. 12, middle), striving to maintain the correct arrangement of the thiophene stacks, followed by an extensive relaxation simulation run that allows the molecules to adjust their arrangement to the best local minimum of free energy. In this simulation, we used the method of Langevin molecular dynamics (LMD), in which the frictional drag or viscous damping term was related to the TCE solvent viscosity (1.484 mPa s at 20 °C). Fig. 14 shows a representative snapshot of the simulated fibril.

During the 20 ns LMD run, certain conformational rearrangement in the fibril occurred, but the structure maintained its integrity and fibrillar shape, so that the supramolecular aggregate can be viewed globally as a nearly linear “super-polymer” exhibiting a large length-to-thickness ratio and characterized by a rather high rigidity. The fibril diameter measured as the distance separating the outermost atoms ranges between 48 and 55 Å, depending on the place where

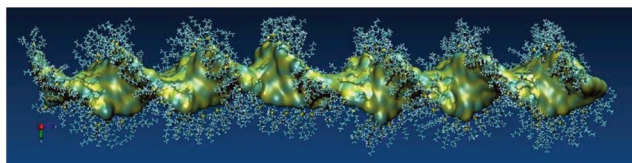


Fig. 14 Snapshot of a helical-like (chiral) supramolecular aggregate formed by 64 structurally symmetric α,ω -substituted oligothiophenes R_3TR_3 in a selective organic solvent. A helicoidal architecture consists of more or less parallel planes or sheets of thiophene blocks which are rotated perpendicular to their long axes in the same direction. The pitch of helicoid is defined as the minimum distance corresponding to a 360° rotation of the direction of the fibril. The diameter of the fibril is about 51 Å. End groups are depicted by sticks, while the inner thiophene core is rendered as a Connolly surface.

measurement is done along the fibril axis; this is comparable to the experimental cross-section of the surface-adsorbed oligothiophene-based fibrils studied by SFM. The fibril has a well pronounced core-shell structure with the shell consisting of alkyl chains that screens the inner thiophene core (Fig. 14). Such a helicoidally organized structure provides more or less good π - π stacking of thiophene rings and, at the same time, a weak overlap of bulky end groups. The shape persistence and rigidity of the helical aggregate are mainly determined by the solvophobicity of oligothiophenes and the strength of π - π stacking. Of course, solvophobic effects are not explicitly taken into account in the LMD simulation, but the attraction between the thiophene rings *per se* along with the van der Waals interactions stabilizes the structure. As in the case of smaller aggregates discussed above, the disintegration of the long fibril is possible only when the terminal molecules split off and go into the solvent.

Discussion

The aggregation curves of the oligothiophene series with various branched substituents display a strong dependence on the concentration and the applied method. UV-vis absorption spectroscopy leads to non-symmetrical curves of $\alpha = f(T)$ with a sudden increase of α with decreasing temperature and a much smoother branch suggesting a cooperative mechanism. This is valid for the whole concentration range between 0.006 and 0.4 mM. Interestingly, the curves become flatter with higher c leading to a physically surprising crossing of the curves. This finding suggests that the assumed strictly linear behaviour between c and absorption, which is the basis for the whole evaluation, is no longer valid. Additionally, extracting the enthalpy from the two regimes (elongation and nucleation) delivers strongly different values which makes the data from absorption measurements at higher concentrations questionable. Still, the cooperative mechanism is supported by DLS measurements although it has to be considered that the scattering intensity is composed of two effects. On one hand, the intensity I should be proportional to the number of aggregates, and on the other hand, it should follow a power law $I \sim r^6$ with the growing size of the aggregates.²⁶ The latter would strongly overestimate the scattering of the aggregates. Thus, the results from DLS have to be considered cautiously, too. Both methods measure the increasing concentration of aggregates. In contrast, from the fluorescence measurements the decrease of the concentration of the oligomers was derived. This shows a similar shape of the curves for low concentration supporting the cooperative behaviour. With increasing concentration, they become much steeper with a sigmoidal shape displaying an apparent change of mechanism to isodesmic aggregation. At low concentration the validity of the Lambert-Beer law can be still assumed, *i.e.*, the fairly coincident curves (Fig. 4) support the cooperative mechanism. With increasing concentration energy loss processes have to be considered like quenching⁴⁰ or energy transfer (*e.g.*, FRET). A broadening of the

emission spectra with increasing concentration supports the assumption of quenching but the ratio of $I_{0-0}(\text{oligomer}) : I_{\text{max}}(\text{aggregate})$ changes from *ca.* 4.5 over 1.6 to 1.3 for $c = 0.006, 0.1$ and 0.4 mM, respectively. This is expected for an energy transfer between oligomers and aggregates, too. On the other hand, a first increase of the intensity of the aggregate emission with lower T is followed by a decrease and subsequent smearing of the isosbestic point. This could be caused by quenching of aggregate emission with increasing concentration of aggregates, too, and would suggest that the change of ratio $I_{0-0}(\text{oligomer}) : I_{\text{max}}(\text{aggregate})$ can also be generated by plain quenching. Both quenching and energy transfer are favoured with smaller intermolecular distances. Although the average distance between single molecules even at $c = 0.4$ mM is far above the van der Waals distances (see Table 1), the presented oligomer/solvent combinations are predestined for such processes as the negative second virial coefficient demonstrates preferred solute–solute over solute–solvent interactions. Thus, pre-aggregation can be assumed favouring energy exchange or loss processes between oligomers and aggregates. The specific form of the effective intermolecular potential calculated by us (see Fig. 11d) confirms the possibility of preliminary aggregation of oligomers in a highly dilute solution. In particular, the existence of the energy barrier and the corresponding local potential minimum of the intermolecular potential can contribute to a weak molecular pre-aggregation, which precedes the subsequent association of oligothiophenes.

The extremely sharp sigmoidal transitions found for the higher concentrations give the opportunity to use the emission characteristics for sensing applications. As described above, there is a steep jump from the aggregated to the non-aggregated state with ΔT between 1.7 and 3.1 K determined at the 0–0 transition and extracted from the fit equation (see the ESI†). The full jump between $\alpha = 1$ and 0 takes place within down to *ca.* 7 K (the steepest slope at $\alpha = 0.5$ for $R_{\text{B}}7\text{TR}_{\text{B}}$ at $c = 0.4$ mM (Fig. 7)). Within this step the emission changes from *ca.* 10^6 to 0 cps. Hence, with an accuracy of the emission measurement of *ca.* 20 000 cps a sensitivity up to 0.14 K can be derived for the determination of the temperature. Furthermore, with the appropriate choice of concentration and molecular structure of the oligomer, the accessible temperature range can be chosen between *ca.* 0 and 100 °C. Thus, the oligomers might act as fully reversible nanothermometers.

The MD simulations performed in this study demonstrate that α,ω -substituted oligothiophenes with flexible-chain aliphatic terminal groups can self-assemble in a selective organic solvent into helical-like (chiral) nanofibrils due to the interplay between the strong π – π attraction of the insoluble oligothiophene blocks and the steric hindrance of the soluble aliphatic chains. The SFM analysis of the adsorbed structures unambiguously reveals the fibrillar morphology of the aggregates. Unfortunately, chirality is not yet supported by an experimental observation since it is quite difficult to elucidate it at the molecular level. We conclude from the simulations that within a single fibril, the vector orientation field is distributed

with a well-pronounced regular twist about the fibril axis. Although each individual fibril is a homochiral object, its “sign of chiral purity” is the result of remembering a random selection of the sign of the small fluctuations occurring in the initial state with the subsequent amplification of this selection. We expect, therefore, that in a macroscopic system, chiral aggregates should form a racemic mixture with equal weights of right-handed and left-handed states and the delta-function-like chirality charge distribution centred at zero. Significant deviations from (macroscopic) zero chirality charge may only result from a strong interaction between neighbouring aggregates. However, this is not possible in solutions. Thus, the hypothesis that the system forms a racemic mixture of chiral fibrils seems plausible.

Conclusions

Oligothiophenes with 7, 9 and 11 thiophene units and branched end-groups display distinctive aggregation in organic solution upon cooling. The oligomers self-assemble into one-dimensional aggregates as revealed by SFM and molecular dynamics simulations. Despite the non-chiral structure of the oligomers, they arrange in helical conformations as derived from the simulations because of the bulky end-groups. The aggregation can be followed by UV-vis absorption, fluorescence emission spectroscopy and DLS. Regardless of the molecular structure at low concentration a non-symmetrical curve is obtained, suggesting a cooperative aggregation mechanism. With increasing concentration, the degree of aggregation derived from UV-vis spectroscopy shows a flattening of the curves still maintaining the cooperative behaviour in agreement with the results from DLS. In contrast, emission spectroscopy displays a change to sigmoidal curves with an apparent switch to “isodesmic” aggregation. Further photophysical experiments would be required to elucidate the origin of the differences. Although fluorescence spectroscopy seems to deliver less reliable results with respect to the aggregation mechanism, it could be highly useful as a nanothermometer. Despite the higher reliability of the absorption measurements, they have to be taken cautiously, too, because of the contradictory behaviour (crossing of the curves and unreliable enthalpy values) especially at high concentrations and low T . Hence, for studies on supramolecular polymerization with higher concentrated solutions a proper adaptation of the method and at least two different methods should be considered to exclude artifacts. If it is possible an upper limit of concentration should not be exceeded. For the present class of compounds this would be in the lower micromolar range.

Conflicts of interest

There are no conflicts to declare.

Acknowledgements

We gratefully acknowledge the support of the present work by the Deutsche Forschungsgemeinschaft (DFG) projects ZI567/4-1 and MO982/2-1. R.V. is thankful for a stipend from the Fonds der Chemischen Industrie. The simulations were carried out using the equipment of the shared research facilities of HPC computing resources at Moscow State University.

Notes and references

- 1 J.-M. Lehn, *Angew. Chem., Int. Ed. Engl.*, 1990, **29**, 1304–1319.
- 2 P. Besenius, *J. Polym. Sci., Part A: Polym. Chem.*, 2017, **55**, 34–78.
- 3 T. Oda, M. Iwasa, T. Aihara, Y. Maeda and A. Narita, *Nature*, 2009, **457**, 441–445.
- 4 A. Faucon, H. Benhelli-Mokrani, F. Fleury, S. Dutertre, M. Tramier, J. Boucard, L. Lartigue, S. Nedellec, P. Hulin and E. Ishow, *Nanoscale*, 2017, **9**, 18094–18106; J. B. Woehrstein, M. T. Strauss, L. L. Ong, B. Wei, D. Y. Zhang, R. Jungmann and P. Yin, *Sci. Adv.*, 2017, **3**, e1602128.
- 5 T. F. A. De Greef, M. M. J. Smulders, M. Wolffs, A. P. H. J. Schenning, R. P. Sijbesma and E. W. Meijer, *Chem. Rev.*, 2009, **109**, 5687–5754.
- 6 M. P. Firestone, R. D. Levie and S. K. Rangarajan, *J. Theor. Biol.*, 1983, **104**, 535–552.
- 7 P. van der Schoot, in *Supramolecular Polymers*, ed. A. Ciferri, Taylor and Francis, Boca Raton, 2005, ch. 3, pp. 77–106.
- 8 M. M. J. Smulders, M. M. L. Nieuwenhuizen, T. F. A. de Greef, P. van der Schoot, A. P. H. J. Schenning and E. W. Meijer, *Chem. – Eur. J.*, 2010, **16**, 362–367.
- 9 J. W. Wackerly and J. S. Moore, *Macromolecules*, 2006, **39**, 7269–7276.
- 10 F. Aparicio, F. Garcia, G. Fernandez, E. Matesanz and L. Sanchez, *Chem. – Eur. J.*, 2011, **17**, 2769–2776.
- 11 A. V. Rudnev, V. L. Malinovskii, A. L. Nussbaumer, A. Mishchenko, R. Haner and T. Wandlowski, *Macromolecules*, 2012, **45**, 5986–5992.
- 12 C. Kulkarni, E. W. Meijer and A. R. A. Palmans, *Acc. Chem. Res.*, 2017, **50**, 1928–1936; A. Das, G. Vantomme, A. J. Markvoort, H. M. M. ten Eikelder, M. Garcia-Iglesias, A. R. A. Palmans and E. W. Meijer, *J. Am. Chem. Soc.*, 2017, **139**, 7036–7044; R. Appel, J. Fuchs, S. M. Tyrrell, P. A. Korevaar, M. C. A. Stuart, I. K. Voets, M. Schonhoff and P. Besenius, *Chem. – Eur. J.*, 2015, **21**, 19257–19264.
- 13 F. Aparicio, F. Garcia and L. Sanchez, *Chem. – Eur. J.*, 2013, **19**, 3239–3248.
- 14 S. Chakraborty, H. Kar, A. Sikder and S. Ghosh, *Chem. Sci.*, 2017, **8**, 1040–1045.
- 15 A. Rodle, B. Ritschel, C. Muck-Lichtenfeld, V. Stepanenko and G. Fernandez, *Chem. – Eur. J.*, 2016, **22**, 15772–15777.
- 16 N. K. Allampally, A. Florian, M. J. Mayoral, C. Rest, V. Stepanenko and G. Fernandez, *Chem. – Eur. J.*, 2014, **20**, 10669–10678.
- 17 R. van der Weegen, A. J. P. Teunissen and E. W. Meijer, *Chem. – Eur. J.*, 2017, **23**, 3773–3783.
- 18 D. van der Zwaag, P. A. Pieters, P. A. Korevaar, A. J. Markvoort, A. J. H. Spiering, T. F. A. de Greef and E. W. Meijer, *J. Am. Chem. Soc.*, 2015, **137**, 12677–12688.
- 19 P. Jonkheijm, P. van der Schoot, A. P. H. J. Schenning and E. W. Meijer, *Science*, 2006, **313**, 80–83.
- 20 F. Würthner, *Acc. Chem. Res.*, 2016, **49**, 868–876.
- 21 R. Schmidt, S. Uemura and F. Würthner, *Chem. – Eur. J.*, 2010, **16**, 13706–13715.
- 22 E. Krieg, H. Weissman, E. Shimoni, A. B. On and B. Rybtchinski, *J. Am. Chem. Soc.*, 2014, **136**, 9443–9452.
- 23 T. Ikeda and T. Haino, *Polymer*, 2017, **128**, 243–256; T. Ikeda, H. Adachi, H. Fueno, K. Tanaka and T. Haino, *J. Org. Chem.*, 2017, **82**, 10062–10069.
- 24 S. Samanta and D. Chaudhuri, *J. Phys. Chem. Lett.*, 2017, **8**, 3427–3432.
- 25 S. Ellinger, A. Kreyes, U. Ziener, C. Hoffmann-Richter, K. Landfester and M. Möller, *Eur. J. Org. Chem.*, 2007, 5686–5702; S. Ellinger, U. Ziener, U. Thewalt, K. Landfester and M. Möller, *Chem. Mater.*, 2007, **19**, 1070–1075.
- 26 A. Kreyes, M. Amirkhani, I. Lieberwirth, R. Mauer, F. Laquai, K. Landfester and U. Ziener, *Chem. Mater.*, 2010, **22**, 6453–6458.
- 27 A. Kreyes, A. Mourran, Z. Hong, J. Wang, M. Möller, F. Gholamrezaie, W. S. C. Roelofs, D. M. de Leeuw and U. Ziener, *Chem. Mater.*, 2013, **25**, 2128–2136.
- 28 J. Gülcher, R. Vill, M. Braumüller, K. Rahimi, W. H. de Jeu, A. Mourran and U. Ziener, *Eur. J. Org. Chem.*, 2017, 1727–1735.
- 29 J. Bicerano, *Prediction of Polymer Properties*, Marcel Dekker Inc., New York, 2002.
- 30 W. H. de Jeu, K. Rahimi, U. Ziener, R. Vill, E. M. Herzig, P. Muller-Buschbaum, M. Moller and A. Mourran, *Langmuir*, 2016, **32**, 1533–1541.
- 31 O. A. Gus'kova, P. G. Khalatur and A. R. Khokhlov, *Macromol. Theory Simul.*, 2009, **18**, 219–246; A. K. Shaytan, A. R. Khokhlov and P. G. Khalatur, *Soft Matter*, 2010, **6**, 1453–1461; A. K. Shaytan, E.-K. Schillinger, P. G. Khalatur, E. Mena-Osteritz, J. Hentschel, H. G. Börner, P. Bäuerle and A. R. Khokhlov, *ACS Nano*, 2011, **5**, 6894–6909; A. K. Shaytan, E. K. Schillinger, E. Mena-Osteritz, S. Schmid, P. G. Khalatur, P. Bäuerle and A. R. Khokhlov, *Beilstein J. Nanotechnol.*, 2011, **2**, 525–544.
- 32 H. Sun, *Macromolecules*, 1995, **28**, 701–712; H. Sun, *J. Phys. Chem. B*, 1998, **102**, 7338.
- 33 M. Blanco, *J. Comput. Chem.*, 1991, **12**, 237–247.
- 34 S. Plimpton, *J. Comput. Phys.*, 1995, **117**, 1–19; LAMMPS package: <http://lammps.sandia.gov> (accessed May 2018).
- 35 S. Hotta and K. Waragai, *Adv. Mater.*, 1993, **5**, 896–908.
- 36 L. E. Hough, M. Spannuth, M. Nakata, D. A. Coleman, C. D. Jones, G. Dantlgraber, C. Tschierske, J. Watanabe,

1	E. Körblova, D. M. Walba, J. E. MacLennan, M. A. Glaser and N. A. Clark, <i>Science</i> , 2009, 325 , 452–456.	39	H.-G. Elias and K. Šolc, <i>Makromol. Chem.</i> , 1975, 176 , 365–371; P. Alexandridis and B. Lindman, <i>Amphiphilic Block Copolymers: Self-Assembly and Applications</i> , Elsevier, Amsterdam, 2000.	1
37	M. Horsch, Z. Zhang and S. Glotzer, <i>Phys. Rev. Lett.</i> , 2005, 95 , 056105.	40	K. P. L. Kuijpers, C. Bottecchia, D. Cambie, K. Drummen, N. J. Konig and T. Noel, <i>Angew. Chem., Int. Ed.</i> , 2018, 57 , 11278–11282.	5
5	38 Y. A. Kriksin and P. G. Khalatur, <i>Macromol. Theory Simul.</i> , 2012, 21 , 382–399.			5
10				10
15				15
20				20
25				25
30				30
35				35
40				40
45				45
50				50
55				55